PFC/RR-88-4

DOE/ET-51013-249
UC 420, 427

Evolution of Poloidal Variation of Impurity Density and Ambipolar Potential in Rotating Tokamak Plasma Part II

Zanino, R. †

March 1988

Plasma Fusion Center
Massachusetts Institute of Technology
Cambridge (MA) 02139 USA

† Present address: Dipartimento di Energetica, Politecnico, Torino, Italy
and
Max-Planck Institut für Plasmaphysik, EURATOM Association
D 8046 Garching, Federal Republic of Germany

ABSTRACT

We present numerical results of a 1-D (poloidal), time dependent code for the description of ion impurity transport on a given tokamak magnetic surface, in the presence of momentum sources such that, as observed in neutral beam injection experiments, the toroidal rotation velocities be comparable to or larger than the impurity thermal speed. We show that the densities, the velocities and the ambipolar potential reach a quasi steady state characterized by significant poloidal gradients, on a time scale of the order of the collision time, i.e. faster than the radial diffusion scale. To obtain this steady state a phenomenological drag force needs be introduced; we find that a purely classical, gyroviscous force alone is apparently insufficient to obtain a steady state, within the framework of the present model which retains only the zero-th order, in the Larmor radius expansion, ion-impurity friction.

1.Introduction

We consider here a two ion components tokamak plasma (index j=i,Z), where "i" indicates the main ion species and "Z" an impurity; impurities are heavier and have a charge Z higher than the charge of the main ions. The relative concentration of the two species is taken as

$$\alpha \equiv n_Z Z^2/n_i \sim O(1)$$

according to the situation in present day experiments, where $Z_{eff} \approx 1+\alpha \geq 2$ is frequently observed . The plasma is toroidally rotating with velocities

$$v_{th,Z} \leq v_{\phi i} \sim v_{\phi Z} < v_{th,i}$$

which are typical for NBI experiments [3].

We are, for the moment, interested in phenomena which happen on a time scale faster than the time scale for radial diffusion, so that no radial transport is considered here. However, we check *a posteriori* the extent to which this assumption is consistent and justifiable (see Section 2.1).

Due to the high toroidal velocities, the inertial (centrifugal and other) forces need be retained in the analysis; these forces act differently on ions and impurities due to the mass difference between the two, and must be balanced by pressure and electric potential *poloidal* gradients arising on every magnetic surface. These surfaces are then no more equipotential.

Also the viscous forces play an important role in this problem: parallel viscosity is needed to damp flows in poloidal direction, but cannot balance any source of toroidal angular momentum; to this purpose a number of different mechanisms has been suggested , among which classical gyroviscosity [4].

The purpose of the present study is to determine the equilibrium resulting from the fast time scale evolution, i.e. the poloidal distributions, for both ion species, of the densities n_j and of the the parallel velocities $V_{\|j}$, together with the self consistent evaluation of the radial electric field E_ψ. (The coupling with the radial transport problem on the slower radial diffusion time scale will be the object of a subsequent paper.)

We have given elsewhere [1] the detailed derivation of a neoclassical fluid model of the problem at hand. The model consists of the continuity equations and the parallel (to **B**)

momentum balances for each of the two ion species, together with the total, flux surface averaged, momentum balance in the diamagnetic ($\mathbf{B} \times \nabla\psi$) direction. This last equation becomes, using the radial momentum balances, the equation for E_ψ - a flux surface quantity to this order. The electrons enter the description of the system in the determination of the parallel electric field, by imposing the quasi-neutrality condition. The temperatures are taken as equal and constant on the surface. For the purpose of simplicity a set of circular, concentric magnetic surfaces is assumed given. The geometrical toroidicity effects, and the nonlinearities arising from the inertial forces $m_j n_j \mathbf{v_j} \cdot \nabla \mathbf{v_j}$ have been fully retained.
The Braginskii [5] prescription for the parallel viscous force is used; we extend here our previous model [1], which was limited to the η_0 contributions, by including also the gyro-viscous piece of the viscous tensor.
Numerical results we presented earlier [2] were limited to the Pfirsch-Schlueter (PS) regime of collisionality (appropriate for the impurities), whereas we now implemented a parallel viscosity coefficient [6] which is independent of the collisionality regime; this is required if any comparison with present day experiments is to be done, where the main ions are typically in the Banana-Plateau (BP) regime. We emphasize however that a form of the viscous force that is valid for compressible flows in the low collisionality regime is not yet known. We thus used the general viscosity coefficient together with the Braginskii functional form, which is rigourously valid only in the PS regime.

In Section 2 the numerical results are presented: in Section 2.1 we consider the case when the momentum sources are balanced by a simplified, drag-like sink term, required to reach a steady state on every given magnetic surface; in Section 2.2 the classical, gyroviscous force is included, and no phenomenological sink term is present any more.
In Appendix A details are given on a semi-analytical, simplified computation of NBI-like parallel momentum sources. In Appendix B, finally, we give the non dimensional form of the set of equations solved.

2.Results

We present in the following a set of typical results, obtained by numerically solving the set of equations given in Appendix B.

We used a pseudo-spectral (collocation) approximation in the poloidal angle, and the NAG routine D02EAF for the integration to steady state of the resulting set of time dependent ODE's.

The geometry and the system of coordinates we are using are shown in Fig.1.

The parallel momentum source arising from neutral beam injection can be approximately determined in a semi-analytical fashion [7], as discussed in Appendix A.

The specific input parameters chosen refer to a certain extent to the ASDEX tokamak data. We took a magnetic surface with minor radius 0.3 m and major radius 1.64 m, (resulting inverse aspect ratio $\epsilon_0 \approx 0.18$), toroidal field 2.5 T and poloidal field 0.25 T, (both at $\theta = \pm\frac{\pi}{2}$), average electron density $4 \times 10^{19} m^{-3}$, average electron temperature 500 eV; when not explicitely stated otherwise, the NB injected power is taken as 1.33 MW, corresponding to half of the maximum power from NBI on ASDEX. Only the case of injection parallel to the magnetic field has been considered, but the model (at least formally) also contains the possibility of describing the effect of a momentum source in diamagnetic direction.

The impurity is Fe^{XVI}, which adequately represents the average charged state for the range of temperatures, corresponding to the range of beam input powers we are interested in. With the previous choices the i-Z collision time is approximately 600 μs, the main ions are in the BP regime ($\nu_{\star i} \approx 0.4$), and the impurities are in the PS regime ($\nu_{\star Z} \epsilon_0^{3/2} \approx 4.2$). All the results refer to the same initial condition of the system, and to the same total time of observation ($t_{TOT} \approx 5$ ms).

2.1 Sources balanced by a phenomenological drag

The drag frequencies ν_{dj} are taken for both species equal to the inverse of a (characteristic) measured total momentum confinement time ; unless explicitely stated otherwise, we take ν_{dj} =50 s^{-1}.

Since we are not considering radial transport, we cannot of course follow the transient from zero flow and flat densities to fully developed profiles, because this occurs on the time scale of $\nu_{dj}^{-1} \sim 10 \div 100$ ms, and not on the fast (collision) time scale ($\sim 100 \mu s$) that we are considering. We can nevertheless pick an initial condition as in Fig.5a, with flat density profiles but (large) toroidal flows such as to balance the source *on the average*, for a given

drag. The result is shown in Figs.2 to 7. (Two general remarks about the plots: whenever ambigous the solid line refers to the impurity species, and the dash-dot line to the main ions; there are always 64 (equispaced) points in the space co-ordinate and 9 (quadratically dense near the origin) in time. These nine points are only used for diagnostic purposes, and the number of time steps required for reaching a steady state is much larger - see Fig.8c.)

In Fig.2 the time evolution of the impurity density poloidal profile is given: large sin θ components develop in the initial stage of the transient due to the strong ion-impurity friction ; then a steady state is reached with large cosine components due to the inertial (centrifugal) forces.

The time evolution of the time derivatives of the i and Z densities and parallel velocities at two given poloidal locations ($\theta = \pi/2$ UP and$\theta = \pi$ OUTBOARD) is shown in Fig.3; one sees that a steady state is reached on a time scale of a few collision times.

The corresponding logarithmic plots for the absolute value of the time derivatives are given in Fig.4a; it is interesting to compare them with Fig.4b which refers to the same initial condition but without source and drag. In the presence of sources the quasi equilibrium resulting from the fast transient successively evolves on the slower time scale of the drag.

Figs.5 show the initial and steady state profiles of the (normalized) densities and of the parallel flow velocities: one can notice that the deviation from uniform density on a given magnetic surface is large for the impurities (solid line), and that some friction between the two ion species still survives at steady state.

The evolution to steady state of the radial electric field and of the absolute value of the poloidal flow velocities for the two species is shown in Fig.6, together with the poloidal distribution of the (dimensionless) electric potential $\frac{e\Phi^0}{T}$. Counterstreaming poloidal flows of a few 10 m s^{-1} are seen to obtain at steady state.

For a decomposition of the impurity density (obtained at $t = t_{TOT}$ as a result of the fast transient) of the form

$$n_Z = a_0(1 + \sum_{k=1}^{N}(a_k cos(k\theta) + b_k sin(k\theta))$$

the Fourier amplitudes b_k and a_k are shown in Figs.7a (b_k/a_0) and 7b (a_k/a_0). The existence of (small) sine components - i.e. *up – down asymmetries* - as in Fig.7a, constitutes a substantial difference with respect to the case without sources, which is purely up-down symmetric [2]. From Fig.7b one sees that already at intermediate injection powers cosine modes develop with amplitudes comparable to the zero-th mode amplitude. This fact

clearly makes an analytical approach, which can afford only a few, at most $O(\epsilon_0)$ amplitude modes [4], rather unreliable.

The accuracy of the code in the case without sources has already been reported [2]. Now, in the presence of sources, the total, flux surface averaged ($< >$), toroidal angular momentum is obviously no more a conserved quantity, but the total number of particles for each species still is; this is actually conserved, with 64 points on the poloidal circumference, within a relative error shown in Fig.8a.

As a further check for the case at hand, we take the solution obtained with 64 points on the poloidal circumference as a reference, and we give in Fig.8b the convergence of the absolute value of the relative error in the first cosine (solid line) and sine Fourier amplitudes of the impurity density, as a function of the number of points. The remarkable feature of the exponential convergence of spectral methods is apparently verified. The corresponding computing cost is given in Fig.8c: the solid line gives the CPU time in seconds, required to reach a steady state, on a CRAY-XMP/24; the dashed line gives the total number (in thousands) of calls of the subroutine internal to D02EAF, which computes the right hand side of the ODE system solved. (The time step used in the integration is controlled by the routine so as to satisfy prescribed accuracy requirements.)

Two important questions still need be discussed: 1) how can one justify neglecting radial flows ? and 2) does the model satisfy *ambipolarity*?

Let us consider the total <toroidal angular momentum> balance, and solve for the <radial particle flow> Γ_j. Neglecting radial convection of toroidal angular momentum (which gives a correction of order $\frac{\rho_{\theta j}}{a}(MACH)_j$, even if not intrinsically ambipolar), one gets

$$\Gamma_j = \frac{1}{|e|Z_j}\frac{1}{RB_\theta}\{\frac{\partial}{\partial t} < Rm_j n_j V_{\phi j} > \pm < Rm_i n_i \nu_{iZ}(V_{\phi Z} - V_{\phi i}) >$$

$$-\frac{B_\phi}{B} < R(M_{\|j} - m_j n_j \nu_{dj} V_{\|j}) >\}.$$

Here the minus sign in the friction term applies to the main ions (j=i), the plus sign to the impurities.

As a measure of the inaccuracy introduced by neglecting the radial flows , one can compare the term (that we neglected) containing the radial flow velocity $V_{\psi j}$ in the continuity equation, with the term depending on the poloidal flow (that we kept). Assuming comparable scale lengths for the radial and poloidal derivatives, one sees that neglecting the radial

flows is correct (at least in this equation !) as far as $V_{\psi j} << V_{\theta j}$. In Fig.9a the radial flow velocity of the impurities $\hat{V}_{\psi Z} \equiv \Gamma_Z / < n_Z >$ is given as a function of time; comparison with Fig.6 shows that neglecting the radial flows is at least not inconsistent with the results of the model. (We emphasize that both the poloidal flow velocities of Fig.6 and the radial flow velocity of Fig.9a are not, however, local quantities, but averages on θ in some sense.) As to the second point raised above, one knows (see Ref.1 equation (13b)) that in the absence of momentum sources in the diamagnetic direction, the main ions and the impurities need to satisfy ambipolarity at steady state, while the (classical) radial electron particle flux is negligible. We are however following a transient, so that one can still get deviations from ambipolarity ΔA until the time derivatives are large (see e.g. the first term in the previous formula). Using the previous formula, we build from the results of the code the quantity

$$\Delta A \equiv \frac{|\Gamma_i + Z\Gamma_Z|}{|\Gamma_i|}$$

which obviously gives an indication of the relative deviation from ambipolarity. One sees from Fig.9b, where ΔA is plotted vs. time, that the results of the code reproduce the qualitative arguments mentioned above.

2.2 Sources balanced by classical gyroviscosity

In this second part we set $\nu_{dj} = 0$ and we try to obtain a steady state in the presence of momentum sources, introducing classical gyroviscous forces.

We emphasize however that the structure of gyroviscosity in the BP regime is not rigorously known; we will thus use expressions valid in PS, and heuristically assume that, unlike the η_0 contributions, the gyroviscous contributions ($\eta_{3,4}$) be basically independent of the collisionality regime.

Within a simplified framework it has been shown [4] that *provided sufficiently large up − down asymmetries in the poloidal density variations can be obtained*, it is possible to balance the toroidal torque introduced by the NBI source by means of a purely classical gyroviscous drag.

Our result in Fig.10 (cfr. Fig.2) shows that no steady state is apparently obtained using as a drag classical gyroviscosity alone; this is basically related to the fact that the sine components of the densities obtained as a result of time evolution of the present set of

equations are not those ones required for gyroviscosity to be effective. The reason for the small sine-amplitudes becomes apparent in Fig.11a showing that the parallel ion and impurity velocities are practically equal, thus almost annihilating the parallel friction. But it is this friction term which generates a finite sinusoidal density variation. If the friction were calculated through first order in the (poloidal) gyroradius expansion, one would expect a finite amplitude for the sin θ density amplitude [10]. The present equations contain only the zero-th order expression for the friction.

Within the present formalism one can compare Fig.11a, which gives the final parallel velocity profiles, with Fig.11b, which gives the profiles for the case when the source is the same but neither drag nor gyroviscosity are present. The two plots are the same, so that classical gyroviscosity is completely ineffective as slowing down torque against the parallel momentum input.

To be sure that no saturation appeared observing the system for a longer time, we have run the code until the main ions parallel velocity reaches the ion thermal speed.

Acknowledgements

The author wishes to thank C.T.Hsu for discussions , K.Lackner and D.J.Sigmar for expert guidance and a critical reading of the manuscript, and the Plasma Fusion Center at MIT for its kind hospitality during the last phase of this work.

All the computations were performed on the CRAY computer at the Max-Planck-Institut fuer Plasma Physik, in Garching, W.Germany.

Appendix A. Semi-analytical, simplified computation of the parallel momentum source due to NB injection

Following Ref.10 we compute here the parallel momentum input due to NBI, on both the main ions and the impurities, for several NBI powers. (We remark that Ref.10 strictly speaking considers the case of toroidal injection, therefore not exactly coincident with the parallel one.)

Taking $\alpha = 1$, and observing that this source term actually comes from a friction process with a third species - the fast beam ions - that we do not consider separately in our model, it is clear that the input on both ion species will be the same.

Part of the momentum input goes directly to the electrons; however we do not take into account sources in the electron parallel momentum balance, assuming they are balanced exactly by e-i and e-Z friction, which are also consistently neglected. In the present calculation this source on the electrons is assumed transferred directly to the ions, equally divided between the two species.

With the notation of Ref.10 we thus have, for arbitrary α

$$M_{\|}^{(i)} = (1 - \frac{\alpha}{\alpha + 1})(M_{\|e} + M_{\|i})$$

and

$$M_{\|}^{(Z)} = \frac{\alpha}{\alpha + 1}(M_{\|e} + M_{\|i}).$$

The two sources are given by

$$M_{\|j} = \dot{n}_f P_{f0} K_j \qquad j = e, i;$$

here

$$\dot{n}_f = \frac{I_o/e}{(2\pi R_0)(\pi a^2)} H(\rho)$$

where $I_o = N_{inj} I_{oo}$, N_{inj} is the (variable) number of NB injector channels, H(ρ) is the spatial shape factor, which should come from a slowing down code (e.g. FREYA [8]), and P_{f0} is the initial fast ion toroidal momentum, depending on the average energy of the source E_0. (For ASDEX N_{inj} can be varied between 1 and 8, $I_{oo} = 15.76$ A, and $E_0 = 25$ keV.)

The K's are plotted in Ref.10 vs. (E_0/E_c), where E_c is the critical energy, dependent on the electron temperature T_e, the ion and beam masses and on α; these plots are given for

various ratios of the i-e scattering time τ_s (dependent also on the electron density n_e) and the charge exchange time

$$\tau_{cx} = \frac{1}{n_{Neutr}\sigma_{cx}V_0}$$

where σ_{cx} is tabulated [9] and depends only on E_0.

To compute the parallel source on any given magnetic surface (ρ = constant) one then needs in principle, for different NB powers P_b (corresponding to different N_{inj}'s) the radial profiles of T_e, n_e, n_{Neutr} and H.

We now assume that $n_e(\rho)$, $n_{Neutr}(\rho)$ and $H(\rho)$ remain constant as P_b varies.(We use in the following $H(\rho = 0.3m) = 0.87$.) Only T_e is allowed to vary following

$$T_e(0) = T_e^{OH}(0) + C\frac{P_b}{< n_e >}$$

where P_b is given in MW and n_e in 10^{13} cm^{-3}, and the temperature radial profiles are taken as simple parabolas without pedestal (in the absence of information on how the temperature at the boundary varies with P_b). In the previous formulas we set T_e^{OH} = 400 eV and C = 4.

We consider the case of deuterium injection into a (mainly) hydrogen plasma. For the foreseen range of T_e, and taking $n_{Neutr}(\rho = 0.3m) = 10^{15}$ m^{-3}, the average impurity ionization state, computed assuming corona equilibrium , grows monotonically with T_e from 15 to 17. We then take, for all P_b, Z = 16.

Table 1 collects, for several injection powers, the different values of $T_e(0)$, $T_e(\rho$= 0.3 m), K_e, K_i, and finally the parallel momentum sources $M_{\|}^{(i)}$ and $M_{\|}^{(Z}$ in N m^{-3}.

Appendix B. Non-dimensional set of equations

We give here the non-dimensional form of the set of equations presented in Ref.1, as it is implemented in the code.

The time coordinate has been non-dimensionalized through the transit time

$$t \longrightarrow \tau \equiv \frac{\mathbf{t}}{\rho/(\beta \mathbf{v_t})} \equiv \omega_t \mathbf{t}$$

where

$$\omega_t \equiv \frac{\beta v_t}{\rho} \qquad \beta \equiv \frac{B_\theta}{B} \qquad v_t \equiv \sqrt{\frac{T}{m_Z}}$$

The dependent functions (unknowns) have been non-dimensionalized according to

$$\mathbf{N_j}(\theta,\tau) \equiv \mathbf{log}(\frac{\mathbf{n_j}(\theta,\mathbf{t})}{\mathbf{n_{i0}}}) \qquad \mathbf{V_j}(\theta,\tau) \equiv \frac{\mathbf{v_{\|j}}(\theta,\mathbf{t})}{\mathbf{v_t}} \qquad \mathbf{V_E}(\tau) \equiv -\frac{\omega(\mathbf{t})\mathbf{R_0}}{\mathbf{v_t}}$$

The momentum sources become

$$S_{\|j}(\theta,\tau) \equiv \frac{M_{\|j}(\theta,t)}{n_j(\theta,t)T/\rho} \qquad S_{\perp j}(\theta,\tau) \equiv \frac{M_{\perp j}(\theta,t)}{n_j(\theta,t)T/\rho}$$

and the collision and drag frequencies

$$\omega_{ij}(N_j) \equiv \frac{\nu_{ij}(n_j)}{\omega_t} \qquad \omega_{dj}^{(\perp)} \equiv \frac{\nu_{dj}^{(\perp)}}{\omega_t}$$

The (local) major radius is

$$R(\theta) = R_0 - \rho cos\theta$$

and consequently the magnetic field components vary with θ as

$$B_\sigma(\theta) = \frac{B_{\sigma 0} R_0}{R(\theta)} \qquad where \qquad B_\sigma = B_\theta, B_\phi \qquad and \qquad B^2 = B_\theta^2 + B_\phi^2$$

The set of equation is thus given by

Continuity:

$$\frac{\partial N_j}{\partial \tau} \quad = \quad -(V_j - \gamma H V_E)\frac{\partial N_j}{\partial \theta} - \frac{\partial V_j}{\partial \theta} - \epsilon sin\theta V_j + 2\gamma\epsilon_0 sin\theta V_E \qquad j = i, Z$$

Main ions parallel momentum:

$$\frac{\partial V_i}{\partial \tau} = \frac{4}{3}\eta_i \frac{\partial^2 V_i}{\partial \theta^2} - (V_i - \gamma H V_E - \frac{4}{3}\eta_i \epsilon sin\theta)\frac{\partial V_i}{\partial \theta}$$

$$-\mu_i(1 + \frac{1}{1+\alpha/Z})\frac{\partial N_i}{\partial \theta} - \mu_i \frac{1}{1+Z/\alpha}\frac{\partial N_Z}{\partial \theta}$$

$$-[\omega_{di} - \gamma\epsilon_0 sin\theta V_E + \eta_i(\frac{1}{3}\epsilon^2 sin^2\theta + \frac{2}{3}\epsilon cos\theta)]V_i$$

$$+\beta^2 H \epsilon_0 sin\theta V_E^2 - \gamma\epsilon_0\eta_i(\epsilon sin^2\theta + \frac{2}{3}cos\theta)V_E + \omega_{iZ}(V_Z - V_i) + \frac{1}{\beta}\mu_i S_{\|i}$$

$$-\eta_{4i}[\frac{V_i}{\hat{\ell}_{Vi}}(\frac{\partial N_i}{\partial \theta} + 4\epsilon sin\theta) - \frac{1}{\hat{\ell}_{Ni}}(\frac{\partial V_i}{\partial \theta} - \epsilon sin\theta V_i)]$$

Impurities parallel momentum:

$$\frac{\partial V_Z}{\partial \tau} = \frac{4}{3}\eta_Z \frac{\partial^2 V_Z}{\partial \theta^2} - (V_Z - \gamma H V_E - \frac{4}{3}\eta_Z \epsilon sin\theta)\frac{\partial V_Z}{\partial \theta}$$

$$-(1 + \frac{Z}{1+Z/\alpha})\frac{\partial N_Z}{\partial \theta} - \frac{Z}{1+\alpha/Z}\frac{\partial N_i}{\partial \theta}$$

$$-[\omega_{dZ} - \gamma\epsilon_0 sin\theta V_E + \eta_Z(\frac{1}{3}\epsilon^2 sin^2\theta + \frac{2}{3}\epsilon cos\theta)]V_Z$$

$$+\beta^2 H \epsilon_0 sin\theta V_E^2 - \gamma\epsilon_0\eta_Z(\epsilon sin^2\theta + \frac{2}{3}cos\theta)V_E + \frac{Z^2}{\mu_i\alpha}\omega_{iZ}(V_i - V_Z) + \frac{1}{\beta}S_{\|Z}$$

$$-\eta_{4Z}[\frac{V_Z}{\hat{\ell}_{VZ}}(\frac{\partial N_Z}{\partial \theta} + 4\epsilon sin\theta) - \frac{1}{\hat{\ell}_{NZ}}(\frac{\partial V_Z}{\partial \theta} - \epsilon sin\theta V_Z)]$$

Total <diamagnetic momentum> :

$$\frac{dV_E}{d\tau} = A_2 V_E^2 - 2A_1 V_E + A_0$$

$$A_2 \equiv \frac{1}{D}\gamma\epsilon_0 \sum_j \frac{m_j}{m_i} < e^{N_j} sin\theta/\epsilon^2 >$$

$$A_1 \equiv \frac{1}{D}\sum_j \{\frac{m_j}{m_i} < e^{N_j} V_j sin\theta/\epsilon > + \frac{1}{2}\frac{m_j}{m_i} < e^{N_j}\omega_{dj}^{\perp}/\epsilon^2 > + \frac{1}{6}\frac{\gamma^2}{\beta^2}\lambda_j < sin^2\theta >\}$$

$$A_0 \equiv \frac{1}{D}\frac{1}{\epsilon_0\beta^2}\{\sum_j \{-\gamma\frac{m_j}{m_i} < e^{N_j} V_j^2 sin\theta > + \frac{1}{3}\gamma\lambda_j < sin\theta(2\frac{\partial V_j}{\partial \theta} - \epsilon sin\theta V_j) >$$

$$-\mu_i < e^{N_j} S_{\perp j}/\epsilon >\} + \gamma\mu_i < [2e^{N_i}\frac{\partial N_i}{\partial\theta} + (1+Z)e^{N_Z}\frac{\partial N_Z}{\partial\theta}]/\epsilon\}$$

$$D \equiv (\frac{1}{\epsilon_0}\frac{c_{Ai}}{c})^2 + \sum_j \frac{m_j}{m_i} < e^{N_j}/\epsilon^2 >$$

Definitions

- $\gamma \equiv \frac{B_\phi}{B}$ $\quad H(\theta) \equiv \frac{R(\theta)}{R_0}$ $\quad \epsilon(\theta) \equiv \frac{\rho}{R(\theta)}$ $\quad \epsilon_0 \equiv \frac{\rho}{R_0}$
- $\alpha = \alpha(N_i, N_Z) \equiv \frac{e^{N_Z} Z^2}{e^{N_i}}$ $\quad \bar{\alpha} \equiv \frac{<e^{N_Z}>Z^2}{<e^{N_i}>}$
- $\omega_{iZ} = \omega_{iZ}(N_Z) \equiv \sqrt{2}\omega_{ii}^{(0)}\alpha e^{N_i}$
- $\eta_j \equiv \gamma\sqrt{(\mu_j/2)}F(\nu_{*j})e^{-N_j}\frac{<n_j>}{n_{i0}}$ $\quad \lambda_j \equiv \frac{m_j}{m_i}e^{N_j}\eta_j$ $\quad \mu_j \equiv \frac{m_Z}{m_j}$

  $F(\nu_{*j}) \equiv \frac{\nu_{*j}}{(1+\nu_{*j})(1+\nu_{*j}\epsilon_0^{\frac{3}{2}})}$ $\quad \nu_{*j} \equiv \frac{\gamma}{\beta}\frac{\rho\nu_j^{tot}}{v_{thj}}\epsilon_0^{-\frac{3}{2}}$

  $\nu_i^{tot} = \nu_{ii}^{(0)}(1+\bar{\alpha}\sqrt{2})$ $\quad \nu_Z^{tot} = \nu_{ii}^{(0)}(\bar{\alpha} + \sqrt{(2/\mu_i)})Z^2/\sqrt{\mu_i}$
- $\eta_{4j} \equiv \frac{\rho_{\theta j}}{\rho}\sqrt{\frac{\mu_j}{2}}$ $\quad \rho_{\theta j} \equiv \frac{m_j v_{thj}}{eZ_j B_\theta}$

  $\hat{\ell}_A^{-1} \equiv \frac{\rho}{A}\frac{\partial A}{\partial \rho}$
- $< X(\theta) > \equiv \frac{\int_0^{2\pi} X(\theta)R(\theta)d\theta}{2\pi R_0}$

References

(1) D.J.Sigmar, R.Zanino, C.T.Hsu, MIT Report PFC/RR-87-8, September 1987

(2) D.J.Sigmar, R.Zanino, C.T.Hsu, *Bull. Am. Phys. Soc.*, Vol.32, 9, 1917, October 1987

(3) K.Brau, *et al.*, Nucl. Fusion, 23, 1643 (1983)

(4) W.M.Stacey, Jr., D.J.Sigmar, Phys. Fluids 27,2076 (1984)

(5) S.I.Braginskii, in *Reviews of Plasma Physics*, edited by M.A.Leontovich (Consultants Bureau, NY, 1965), Vol.1

(6) S.P.Hirshman, Phys. Fluids, 21, 224 (1978)

(7) J.D.Callen, *et al.*, IAEA-CN-33/A16-3, Tokio, 1974

(8) G.G.Lister, *et al.*, Proceedings of the III Meeting on Heating, 303, Varenna, 1973

(9) R.L.Freeman, E.M.Jones, Culham Report CLM-R 137, 1974

(10) C.T.Hsu, D.J.Sigmar, private communication

Figure captions

1) Geometry and co-ordinate system

2) Time evolution of the poloidal impurity density profile

3) Time derivatives of the impurity (solid lines) and main ion densities and parallel flow velocities vs. time, at two poloidal locations ($\theta_{UP} = \pi/2$, $\theta_{OUTBOARD} = \pi$).

4a) Same as 3) but logarithmic scale on the ordinates

4b) Same as 4a) but $M_{\|j} = \nu_{dj} = 0$

5a) Initial poloidal profiles of the (normalized) densities and of the parallel flow velocities of the impurities (solid lines) and of the main ions

5b) Final ($t = t_{TOT}$) poloidal profiles of the (normalized) densities and of the parallel flow velocities of the impurities (solid lines) and of the main ions

6) From upper left clockwise: time derivative of the radial electric field vs. time; radial electric field vs. time; $|K_j(\psi) \equiv \frac{n_j|V_{\theta j}|}{B}\frac{B_0}{<n_j>}$ vs. time, j = i, Z (solid line); $\frac{|e|\Phi^{(0)}}{T}$ vs. time

7a) Sine Fourier amplitudes of n_i and of n_Z (solid line) vs. mode number at $t = t_{TOT}$

7b) Cosine Fourier amplitudes of n_i and of n_Z (solid line) vs. mode number at $t = t_{TOT}$

8a) $\frac{|<n_j(\theta,t_{TOT})>-<n_j(\theta,t=0)>|}{<n_j(\theta,t=0)>}$ vs. time, j = i, Z (solid line)

8b) $\frac{|a_1^{N=NP}-a_1^{N=64}|}{|a_1^{N=64}|}$ (solid line), and $\frac{|b_1^{N=NP}-b_1^{N=64}|}{|b_1^{N=64}|}$ vs. the number of points NP on the poloidal circumference

8c) CPU time on a CRAY-XMP/24 to reach steady state (solid line) and number of calls (in thousands) of the subroutine internal to D02EAF vs. NP

9a) Average radial flow velocity of the impurities vs. time

9b) Relative deviation from ambipolarity vs. time

10) Time evolution of the poloidal impurity density profile, using as a drag against parallel momentum sources gyroviscosity alone

11a) Final parallel flow velocity poloidal profiles, using as a drag against parallel momentum sources gyroviscosity alone

11b) Final parallel flow velocity poloidal profiles (no drag, no gyroviscosity)

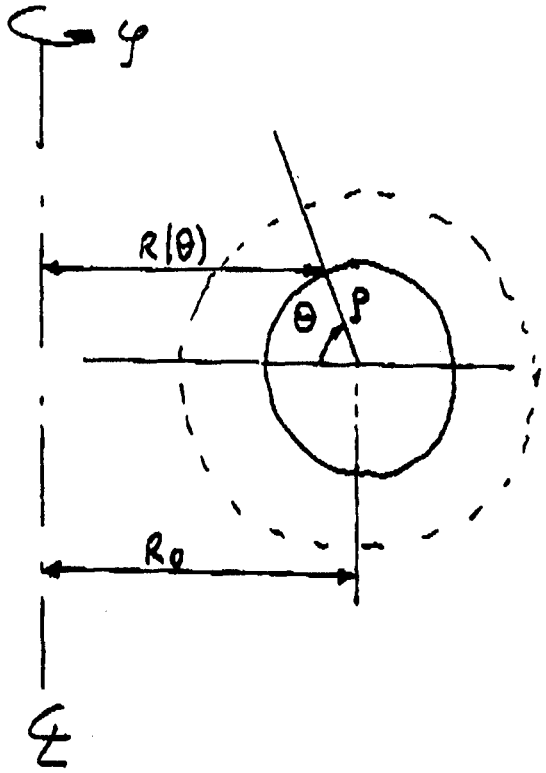

$$\frac{\partial A}{\partial \varphi} = 0 \quad , \quad \forall A \in \mathbb{R}$$

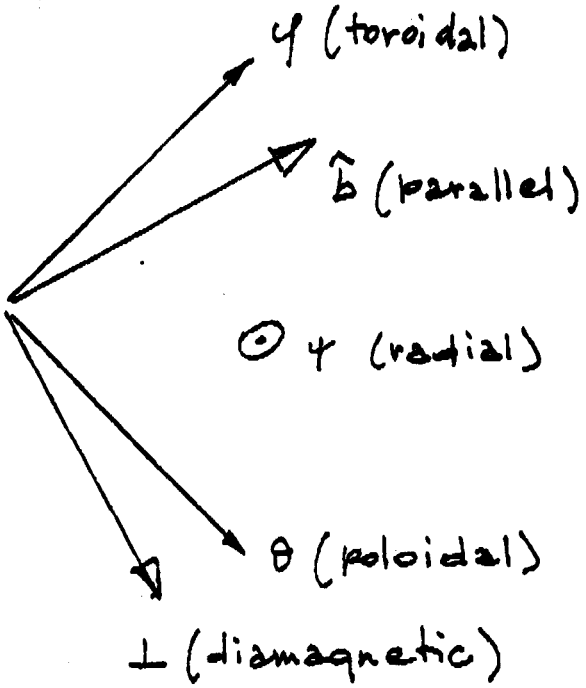

FIG. 1

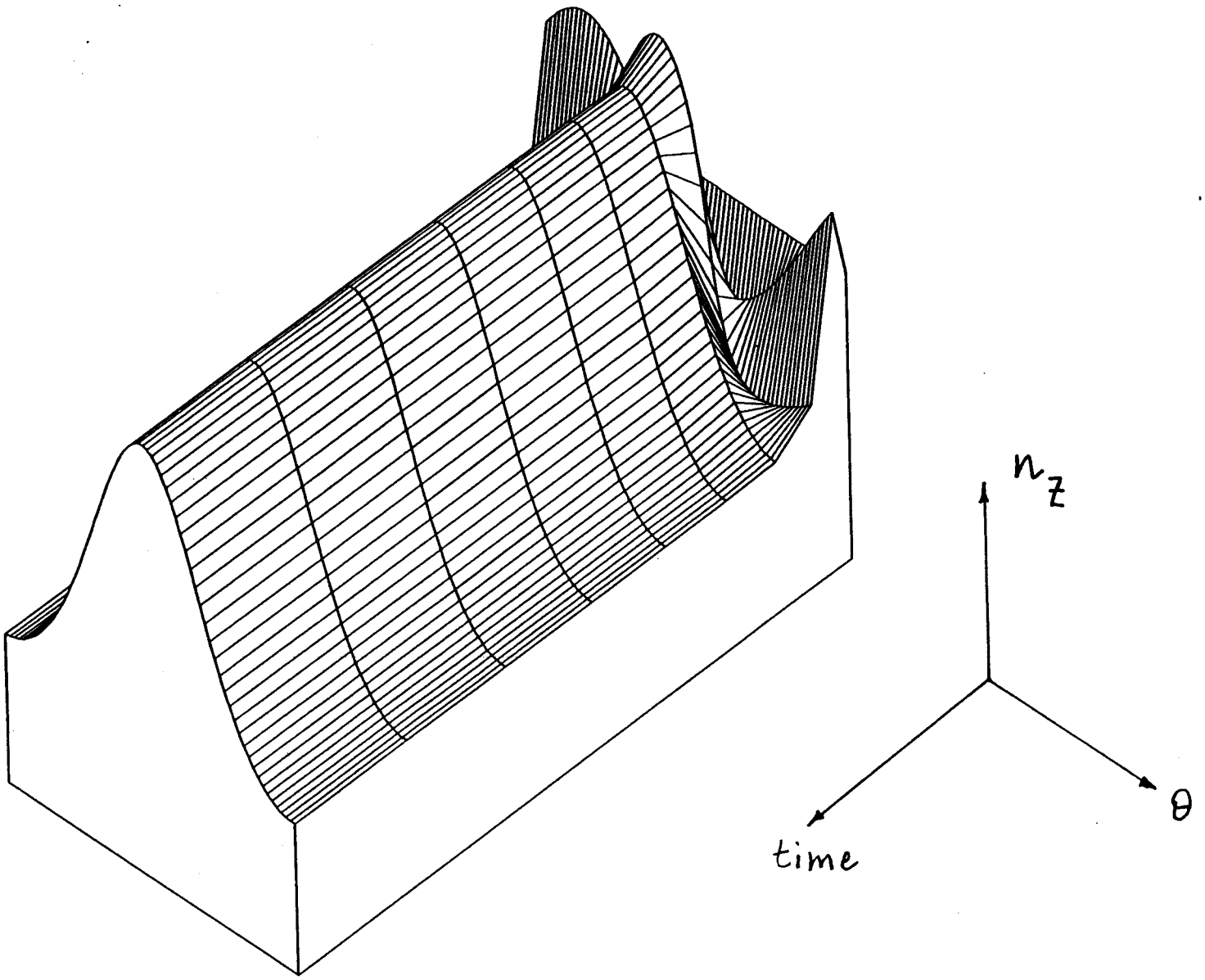

FIG. 2

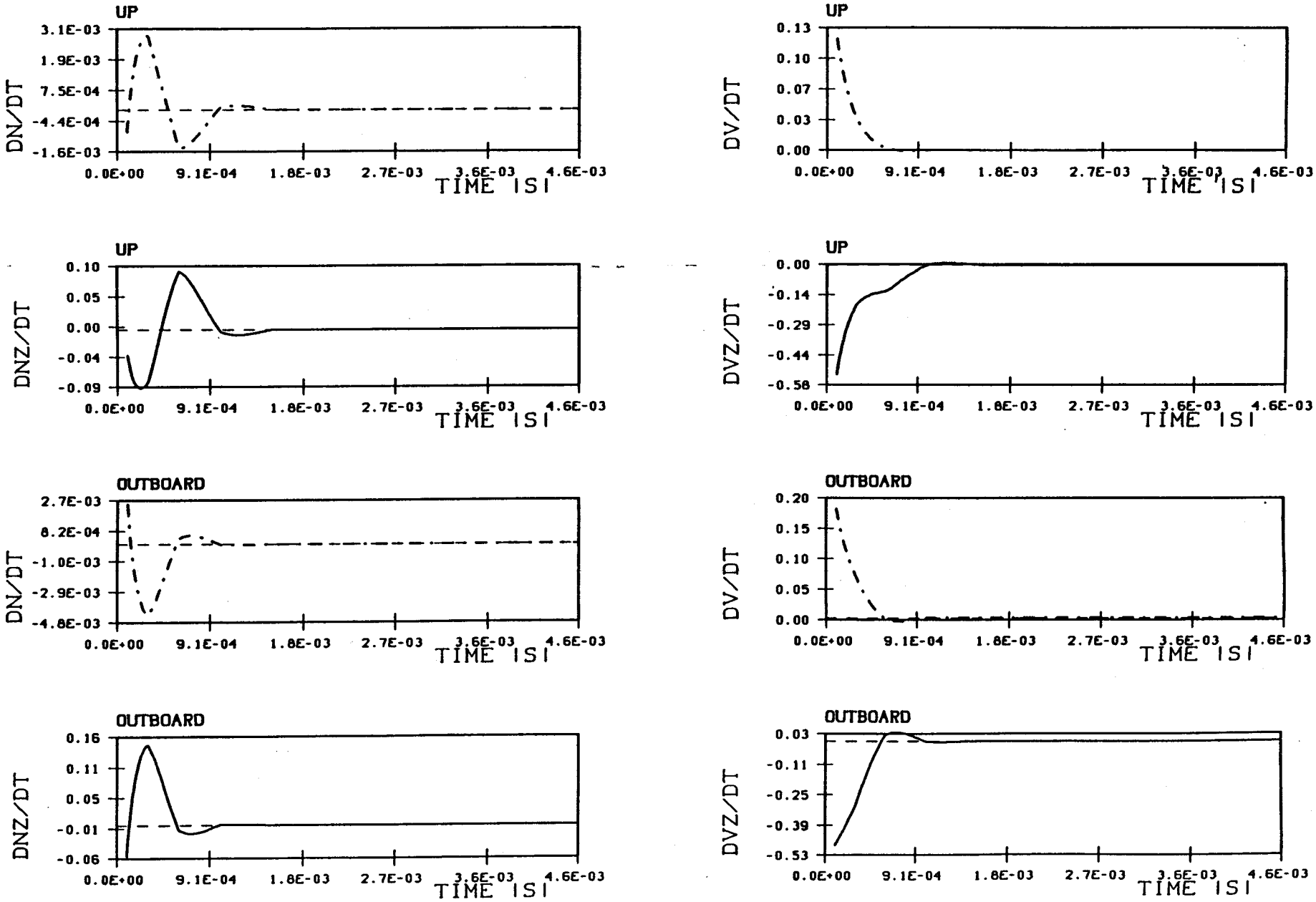
UP
DN/DT
3.1E-03
1.9E-03
7.5E-04
-4.4E-04
-1.6E-03
0.0E+00
9.1E-04
1.8E-03
2.7E-03
3.6E-03
4.6E-03
TIME ISI
UP
DV/DT
0.13
0.10
0.07
0.03
0.00
0.0E+00
9.1E-04
1.8E-03
2.7E-03
3.6E-03
4.6E-03
TIME ISI
UP
DNZ/DT
0.10
0.05
0.00
-0.04
-0.09
0.0E+00
9.1E-04
1.8E-03
2.7E-03
3.6E-03
4.6E-03
TIME ISI
UP
DVZ/DT
0.00
-0.14
-0.29
-0.44
-0.58
0.0E+00
9.1E-04
1.8E-03
2.7E-03
3.6E-03
4.6E-03
TIME ISI
OUTBOARD
DN/DT
2.7E-03
8.2E-04
-1.0E-03
-2.9E-03
-4.8E-03
0.0E+00
9.1E-04
1.8E-03
2.7E-03
3.6E-03
4.6E-03
TIME ISI
OUTBOARD
DV/DT
0.20
0.15
0.10
0.05
0.00
0.0E+00
9.1E-04
1.8E-03
2.7E-03
3.6E-03
4.6E-03
TIME ISI
OUTBOARD
DNZ/DT
0.16
0.11
0.05
-0.01
-0.06
0.0E+00
9.1E-04
1.8E-03
2.7E-03
3.6E-03
4.6E-03
TIME ISI
OUTBOARD
DVZ/DT
0.03
-0.11
-0.25
-0.39
-0.53
0.0E+00
9.1E-04
1.8E-03
2.7E-03
3.6E-03
4.6E-03
TIME ISI

FIG. 3

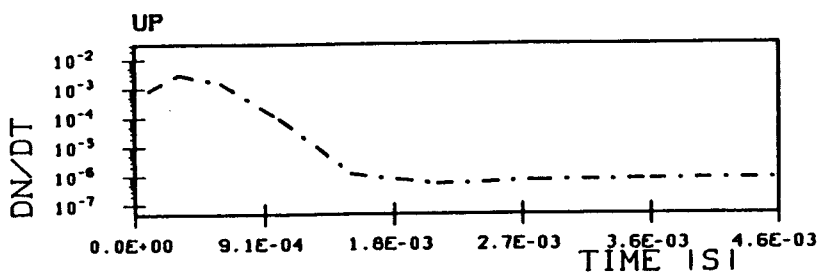
UP
DN/DT
10^{-2}
10^{-3}
10^{-4}
10^{-5}
10^{-6}
10^{-7}
0.0E+00
9.1E-04
1.8E-03
2.7E-03
3.6E-03
4.6E-03
TIME (S)

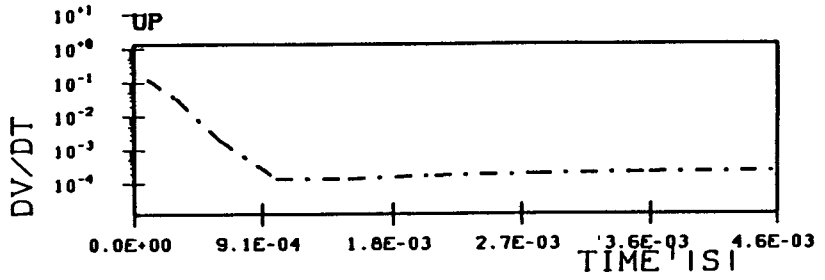
UP
DV/DT
10^{+1}
10^{+0}
10^{-1}
10^{-2}
10^{-3}
10^{-4}
0.0E+00
9.1E-04
1.8E-03
2.7E-03
3.6E-03
4.6E-03
TIME (S)

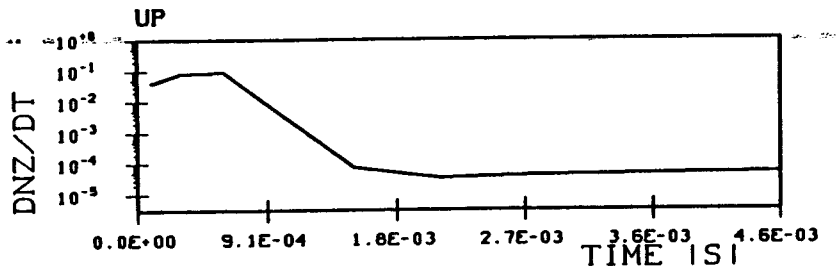
UP
DNZ/DT
10^{+0}
10^{-1}
10^{-2}
10^{-3}
10^{-4}
10^{-5}
0.0E+00
9.1E-04
1.8E-03
2.7E-03
3.6E-03
4.6E-03
TIME (S)

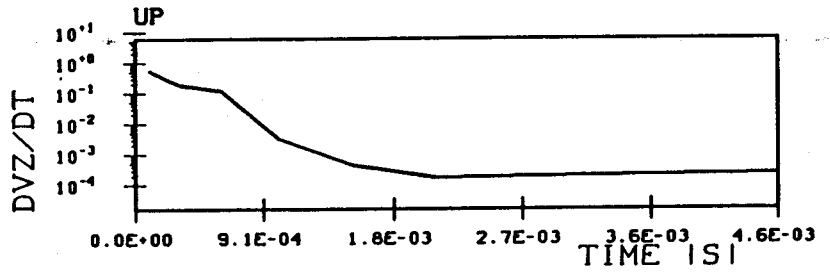
UP
DVZ/DT
10^{+1}
10^{+0}
10^{-1}
10^{-2}
10^{-3}
10^{-4}
0.0E+00
9.1E-04
1.8E-03
2.7E-03
3.6E-03
4.6E-03
TIME (S)

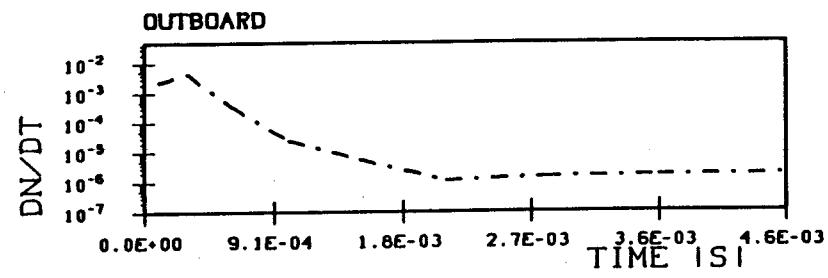
OUTBOARD
DN/DT
10^{-2}
10^{-3}
10^{-4}
10^{-5}
10^{-6}
10^{-7}
0.0E+00
9.1E-04
1.8E-03
2.7E-03
3.6E-03
4.6E-03
TIME (S)

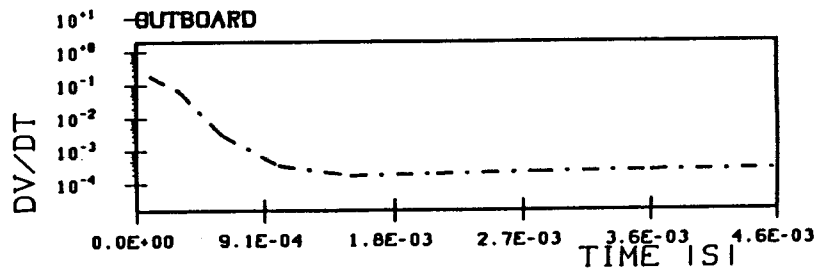
OUTBOARD
DV/DT
10^{+1}
10^{+0}
10^{-1}
10^{-2}
10^{-3}
10^{-4}
0.0E+00
9.1E-04
1.8E-03
2.7E-03
3.6E-03
4.6E-03
TIME (S)

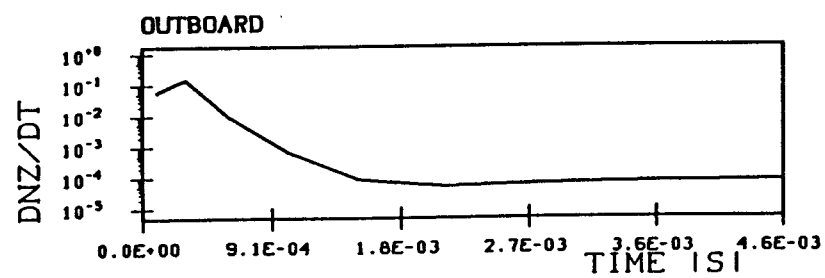
OUTBOARD
DNZ/DT
10^{+0}
10^{-1}
10^{-2}
10^{-3}
10^{-4}
10^{-5}
0.0E+00
9.1E-04
1.8E-03
2.7E-03
3.6E-03
4.6E-03
TIME (S)

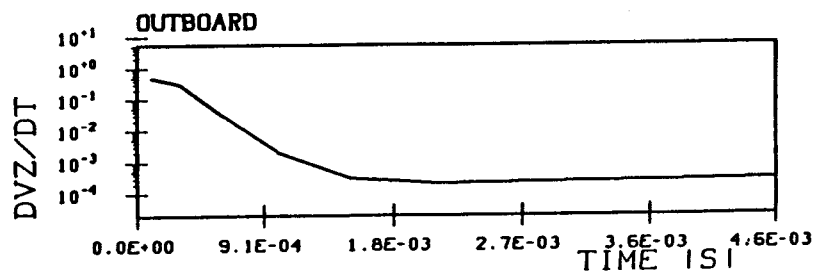
OUTBOARD
DVZ/DT
10^{+1}
10^{+0}
10^{-1}
10^{-2}
10^{-3}
10^{-4}
0.0E+00
9.1E-04
1.8E-03
2.7E-03
3.6E-03
4.6E-03
TIME (S)

FIG. 4a

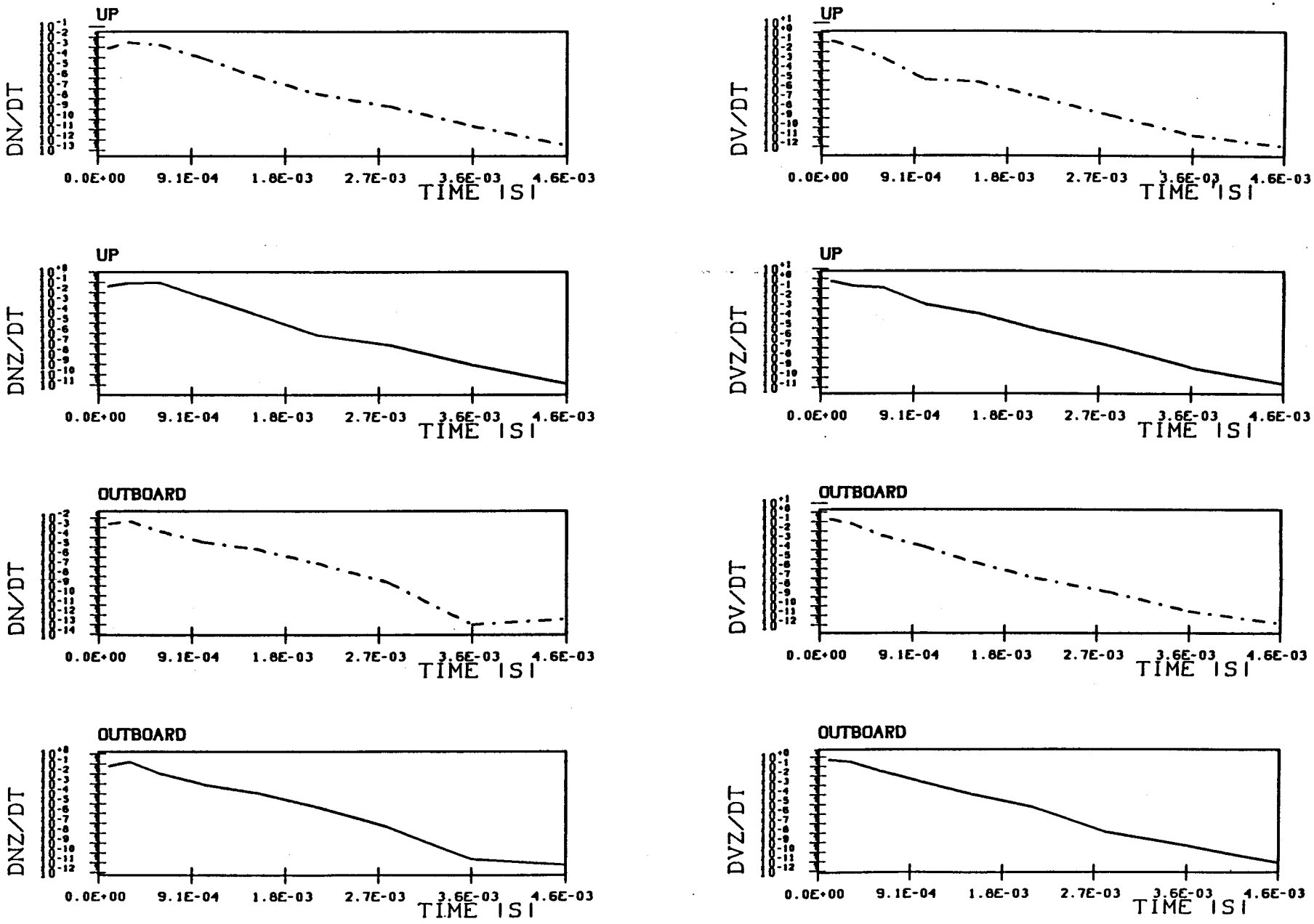
UP
DN/DT
DV/DT
DNZ/DT
DVZ/DT
OUTBOARD
0.0E+00
9.1E-04
1.8E-03
2.7E-03
3.6E-03
4.6E-03
TIME ISI

FIG. 46

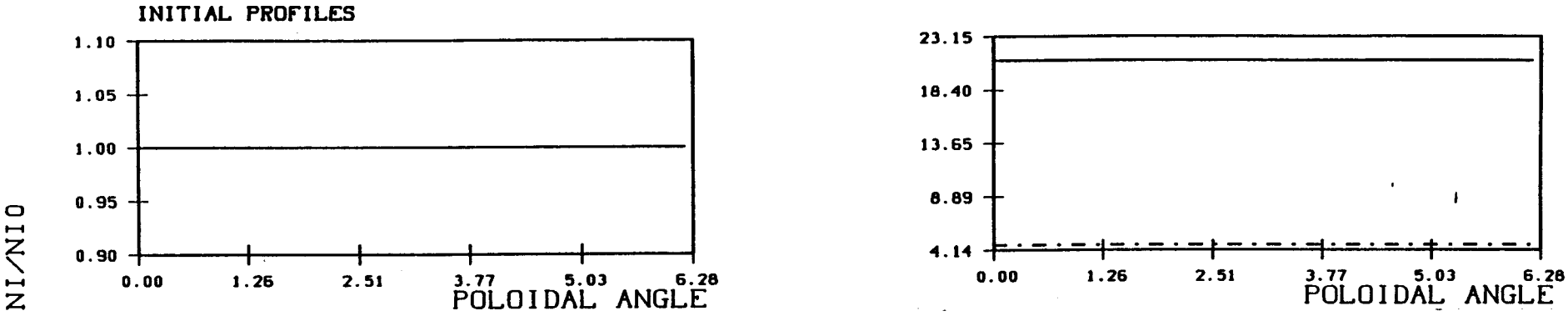
INITIAL PROFILES
NI/NI0
1.10
1.05
1.00
0.95
0.90
0.00
1.26
2.51
3.77
5.03
6.28
POLOIDAL ANGLE
23.15
18.40
13.65
8.89
4.14
0.00
1.26
2.51
3.77
5.03
6.28
POLOIDAL ANGLE

Fig. 5a

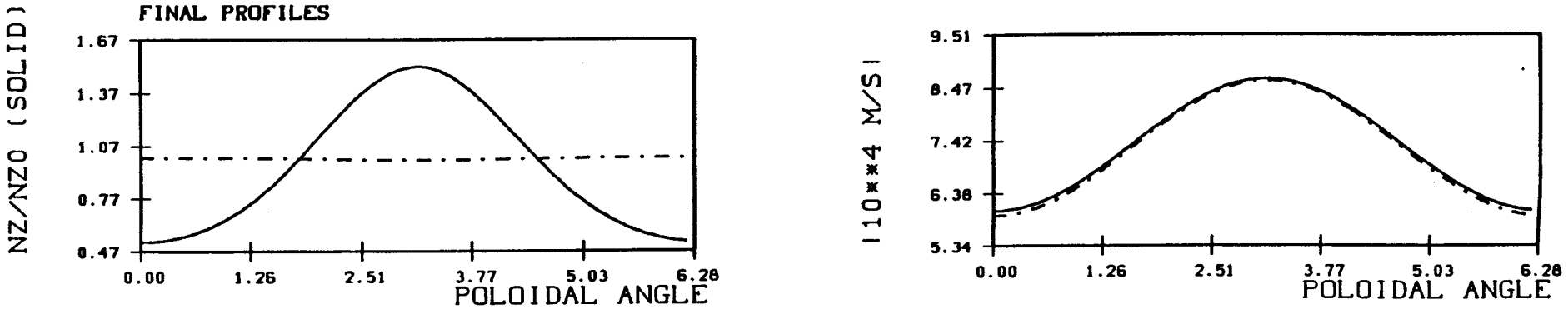
FINAL PROFILES
NZ/NZ0 (SOLID)
1.67
1.37
1.07
0.77
0.47
0.00
1.26
2.51
3.77
5.03
6.28
POLOIDAL ANGLE
I10**4 M/SI
9.51
8.47
7.42
6.38
5.34
0.00
1.26
2.51
3.77
5.03
6.28
POLOIDAL ANGLE

Fig. 5b

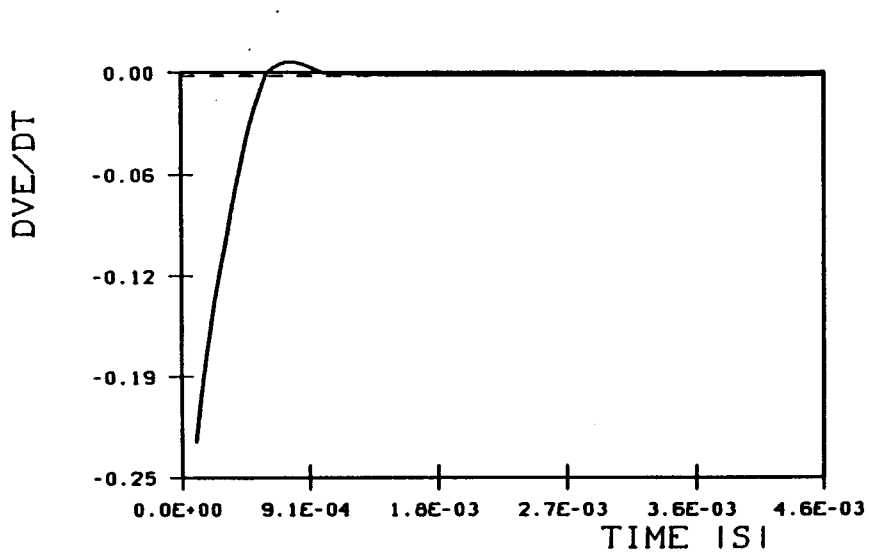
DVE/DT
0.00
-0.06
-0.12
-0.19
-0.25
0.0E+00
9.1E-04
1.8E-03
2.7E-03
3.6E-03
4.6E-03
TIME (S)

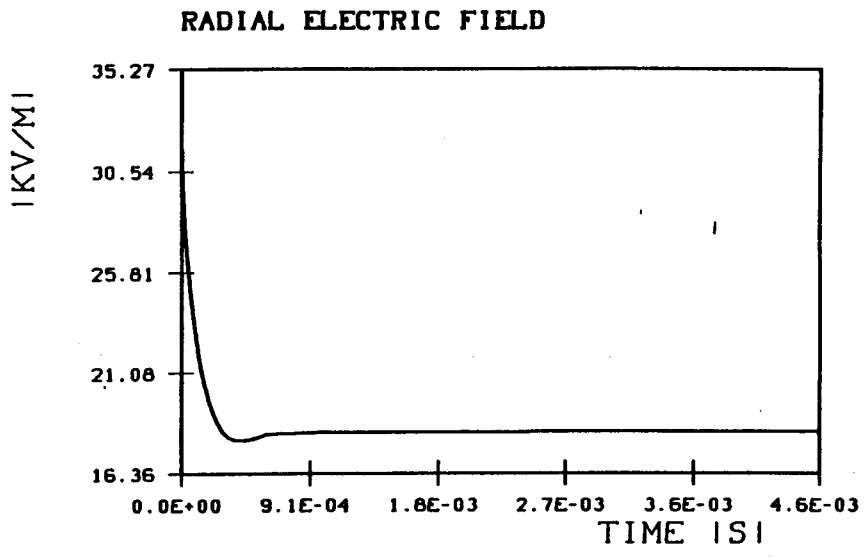
RADIAL ELECTRIC FIELD
(KV/M)
35.27
30.54
25.81
21.08
16.36
0.0E+00
9.1E-04
1.8E-03
2.7E-03
3.6E-03
4.6E-03
TIME (S)

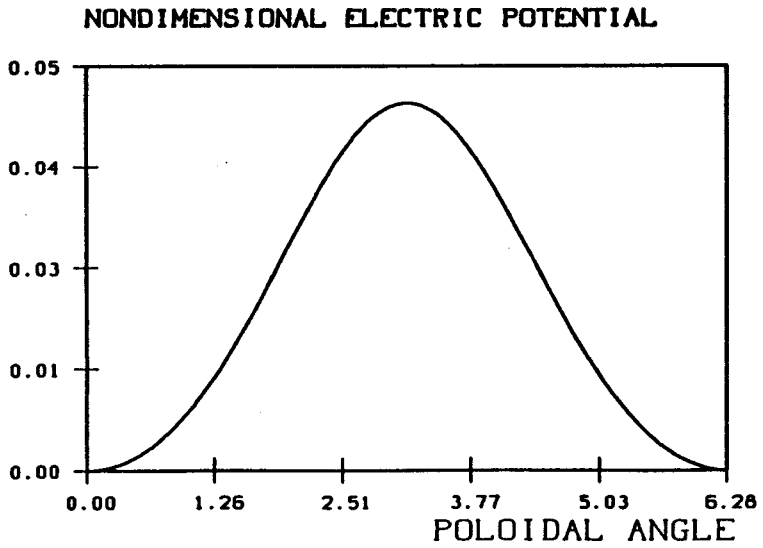
NONDIMENSIONAL ELECTRIC POTENTIAL
0.05
0.04
0.03
0.01
0.00
0.00
1.26
2.51
3.77
5.03
6.28
POLOIDAL ANGLE

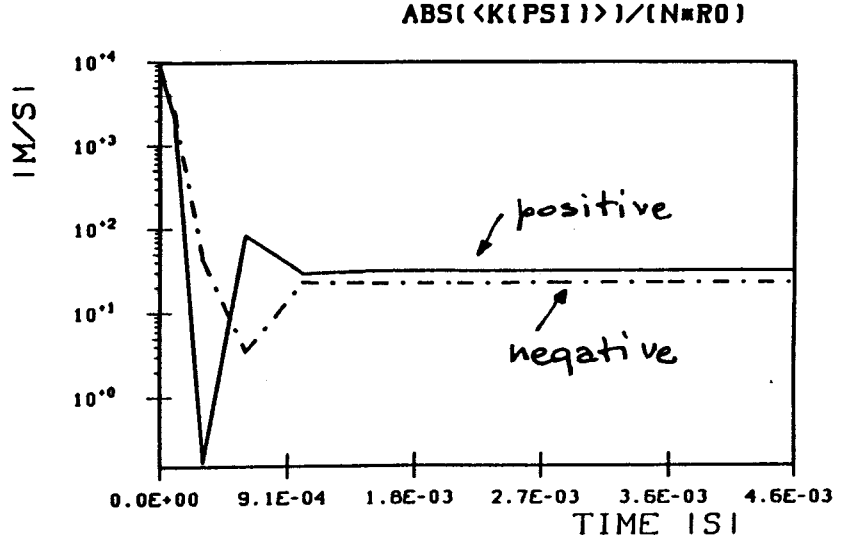
ABS(<K(PSI)>)/(N*R0)
(M/S)
positive
negative
0.0E+00
9.1E-04
1.8E-03
2.7E-03
3.6E-03
4.6E-03
TIME (S)

Fig. 6

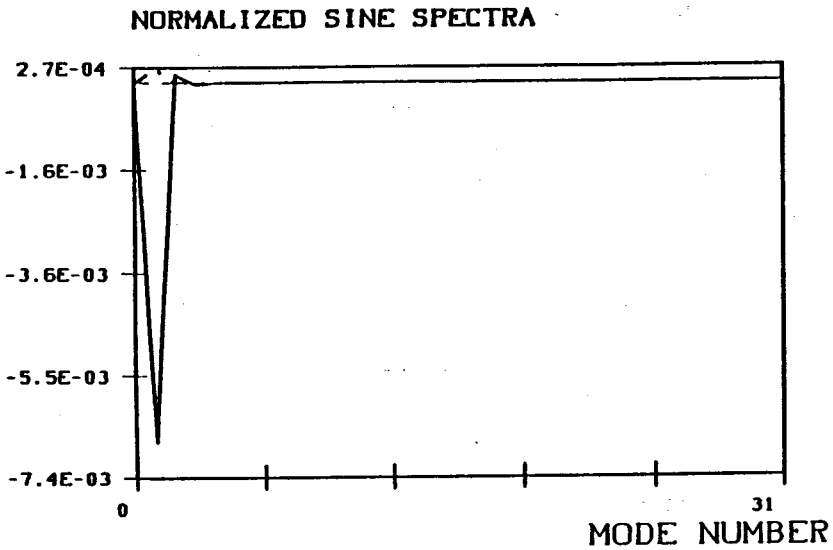
NORMALIZED SINE SPECTRA
2.7E-04
-1.6E-03
-3.6E-03
-5.5E-03
-7.4E-03
0
31
MODE NUMBER

FIG. 7a

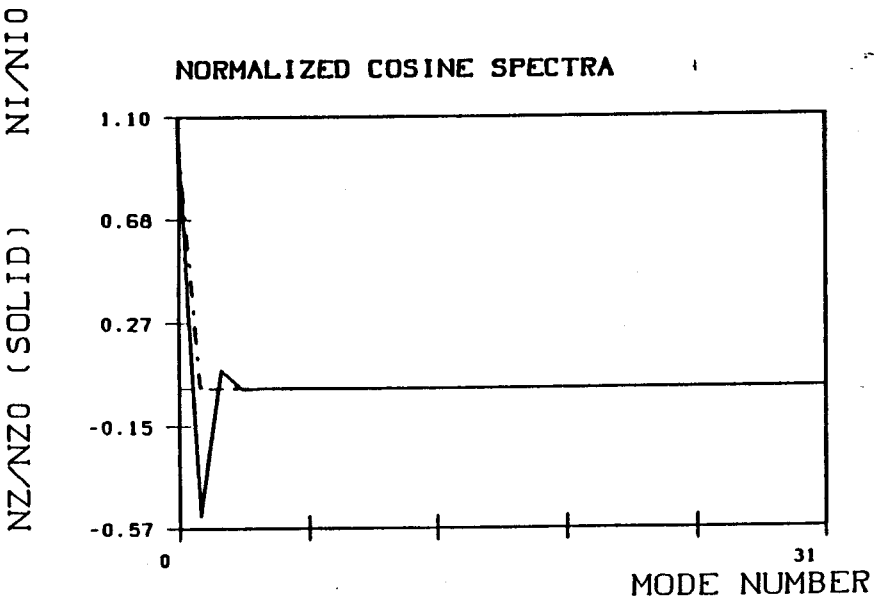
NORMALIZED COSINE SPECTRA
NZ/NZO (SOLID) NI/NIO
1.10
0.68
0.27
-0.15
-0.57
0
31
MODE NUMBER

FIG. 7b

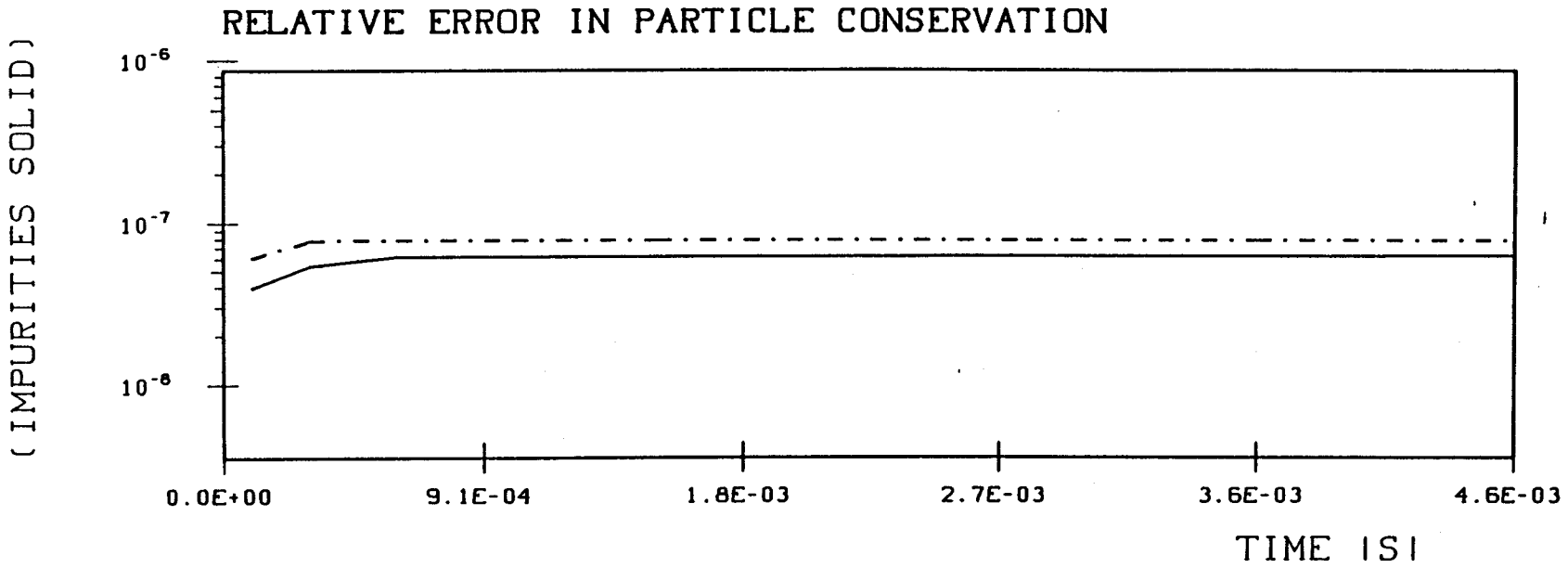
RELATIVE ERROR IN PARTICLE CONSERVATION
(IMPURITIES SOLID)
10-6
10-7
10-8
0.0E+00
9.1E-04
1.8E-03
2.7E-03
3.6E-03
4.6E-03
TIME (S)

FIG. 8a

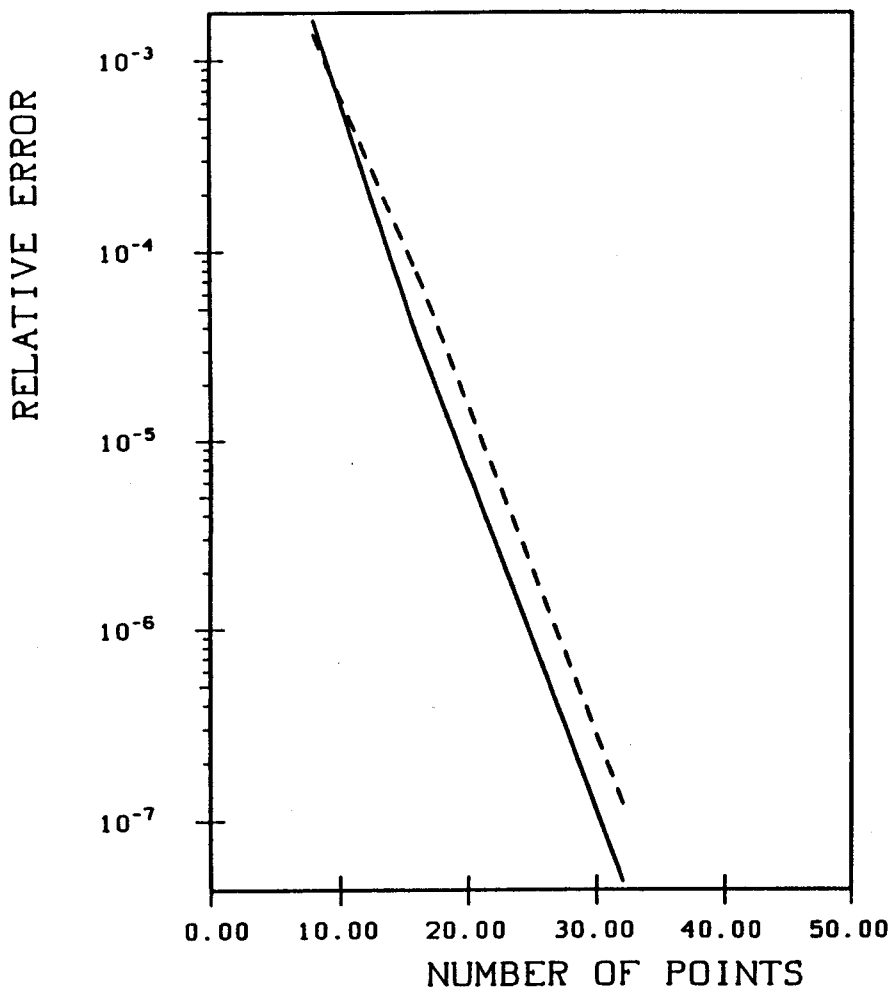
RELATIVE ERROR
10^{-3}
10^{-4}
10^{-5}
10^{-6}
10^{-7}
0.00
10.00
20.00
30.00
40.00
50.00
NUMBER OF POINTS

FIG. 8b

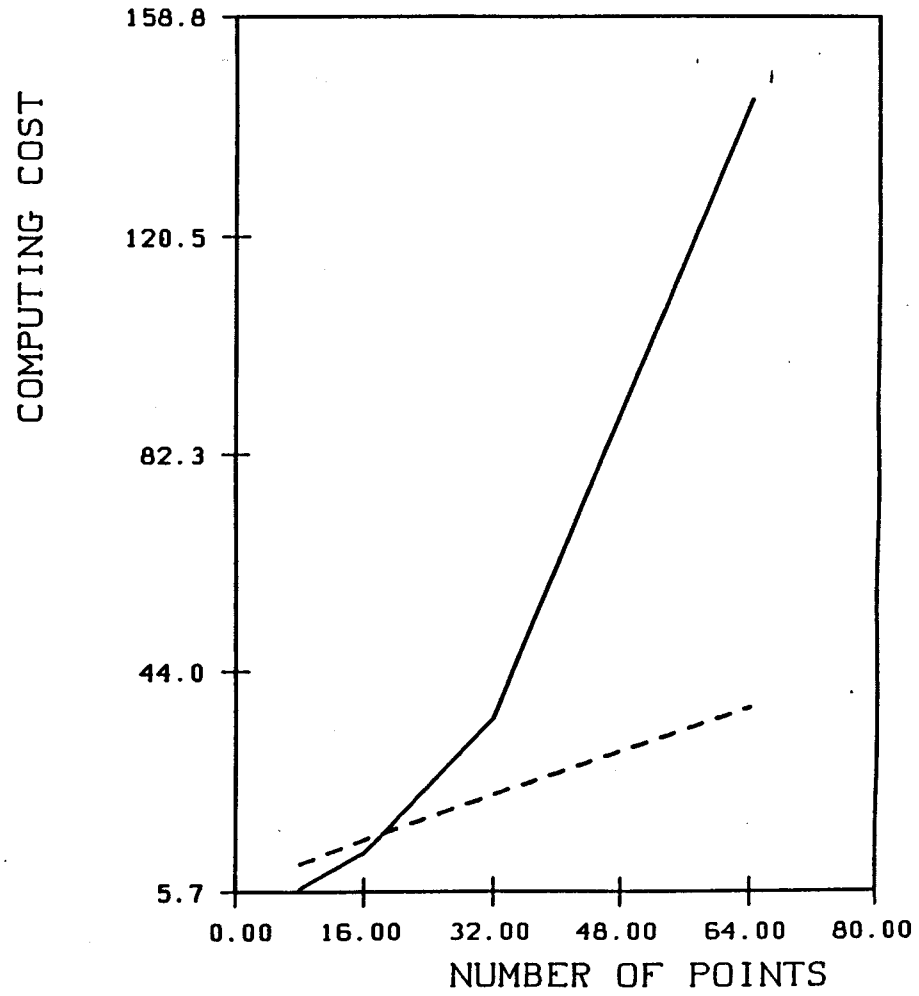
COMPUTING COST
158.8
120.5
82.3
44.0
5.7
0.00
16.00
32.00
48.00
64.00
80.00
NUMBER OF POINTS

FIG. 8c

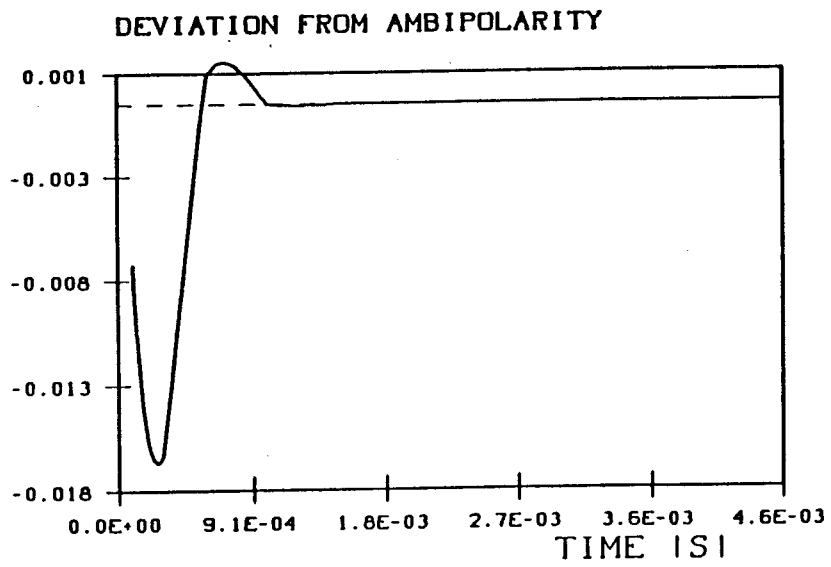
DEVIATION FROM AMBIPOLARITY
0.001
-0.003
-0.008
-0.013
-0.018
0.0E+00
9.1E-04
1.8E-03
2.7E-03
3.6E-03
4.6E-03
TIME (S)

FIG. 9b

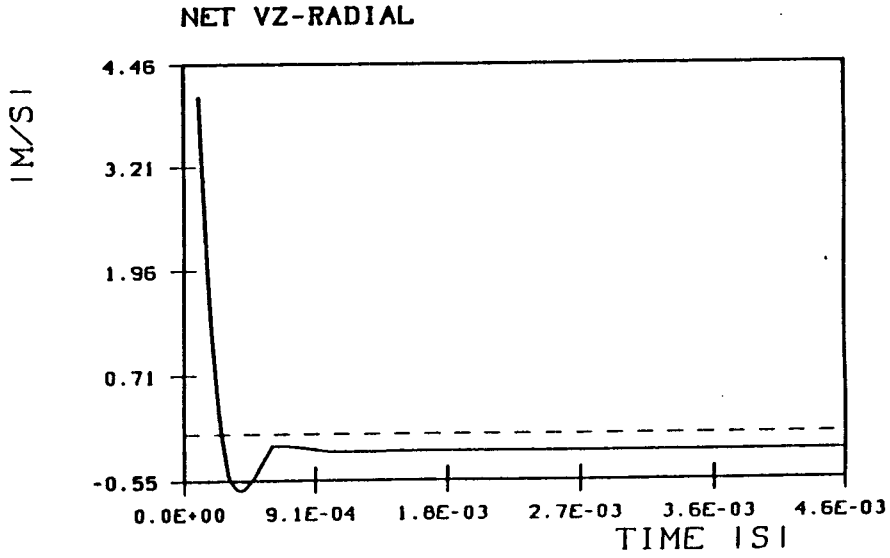
NET VZ-RADIAL
(M/S)
4.46
3.21
1.96
0.71
-0.55
0.0E+00
9.1E-04
1.8E-03
2.7E-03
3.6E-03
4.6E-03
TIME (S)

FIG. 9a

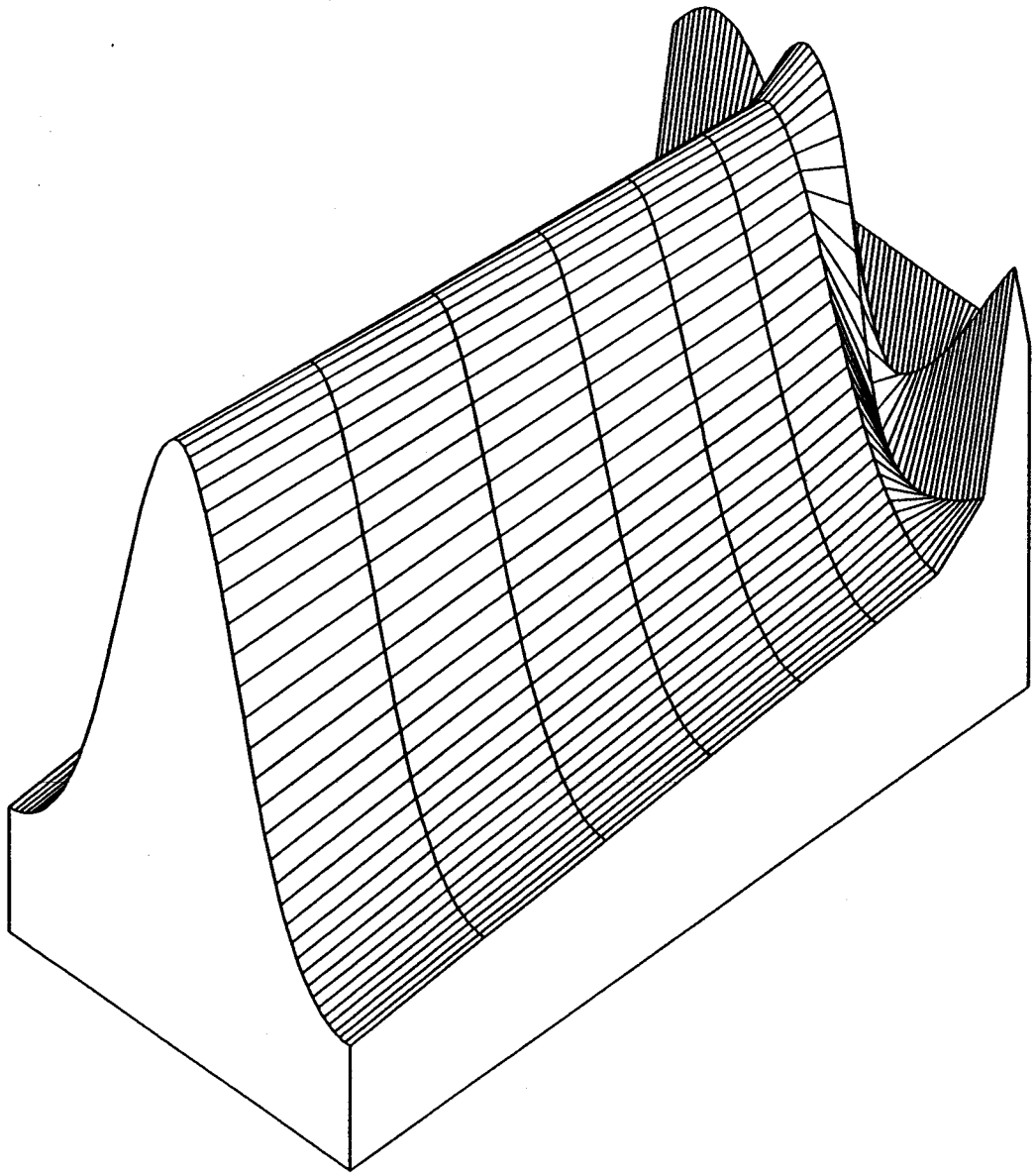

FIG. 10

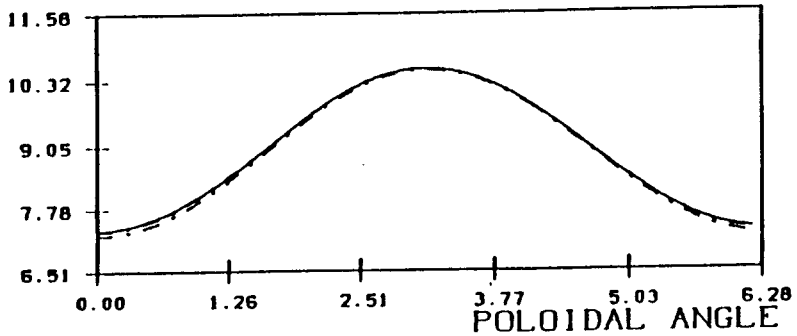

FIG. 11a

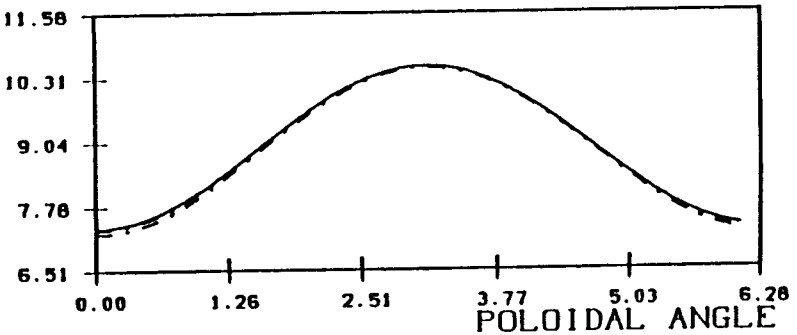

FIG. 11b

P_b [MW]	$T_e(0)$ [eV]	$T_e(\rho = 0.3\ \mathrm{m})$ [eV]	K_e	K_i	$M_{\|\|}$ [N m^{-3}]
0.333	663	290	0.28	0.48	0.046
0.666	930	407	0.22	0.52	0.089
1.333	1463	640	0.16	0.48	0.154
2.000	1993	872	0.10	0.54	0.230
2.666	2526	1105	0.06	0.50	0.269

Table 1